Petroleum Science 19 (2022) 2969–2980

Contents lists available at ScienceDirect

Petroleum Science

journal homepage: www.keaipublishing.com/en/journals/petroleum-science

Original Paper

Effect of the number of irradiation holes on rock breaking under constant laser energy

Hai-Zeng Pan [a, b], Yi Hu [a, c, *], Yong Kang [a, b], Ze-Feng Wang [d, **], Jia-Wei Liu [e], Hao Chen [a, b], Meng-Da Zhang [a, b]

[a] Hubei Key Laboratory of Waterjet Theory and New Technology, Wuhan University, Wuhan, 430072, Hubei, China
[b] School of Power and Mechanical Engineering, Wuhan University, Wuhan, 430072, Hubei, China
[c] The Institute of Technological Sciences, Wuhan University, Wuhan, 430072, Hubei, China
[d] School of Urban Construction, Wuhan University of Science and Technology, Wuhan, 430081, Hubei, China
[e] Jianghan Machinery Research Institute Limited Company of CNPC, Wuhan, 430000, Hubei, China

ARTICLE INFO

Article history:
Received 24 January 2022
Received in revised form
10 June 2022
Accepted 13 June 2022
Available online 15 June 2022

Edited by Yan-Hua Sun

Keywords:
Number of irradiation holes
Rock breaking
Fracture tortuosity
Macrofracture

ABSTRACT

The use of mechanical drilling in accessing energy resources stored in deep and hard rock formations is becoming increasingly challenging. Thus, laser irradiation has emerged as a novel drilling method with considerable in this context. This study examines the variation of rock fracture length, fracture tortuosity, hole size, and rock breaking efficiency for a different number of holes and laser power, based on the constant total energy of laser irradiation. As indicated by the results, increasing the laser power increases the laser intensity, which helps increase the hole diameter and depth. Moreover, for the same laser power, increasing the number of irradiated holes reduces the laser energy absorbed by each hole, which is not conducive to increasing the hole depth. As the number of holes increases, the mass loss of the rock also increases, while both specific energy (SE) and modified specific energy (MSE) decrease. When the number of holes remains the same, the mass of the shale removed by low power is less than that removed by high power, while SE and MSE have an inverse relation with power. Therefore, high laser power and multiple-hole irradiation are more conducive to rock breaking. Besides, the fracture length and fracture tortuosity of the rock irradiated by the low laser power will increase first and then decrease with the increase in the number of holes, and reach the peak value when the irradiation takes place through three holes. When a high-power laser irradiates the rock, the fracture length and tortuosity will increase with the increase in the number of irradiation holes. This is because a rock irradiated by low power dissipates more energy, with the result that the energy absorbed by the sample with four irradiation holes is not enough to break the rock quickly. This study is expected to provide some guidance to break rock for drilling deep reservoirs and hard rock formations using laser irradiation.

1. Introduction

As the exploitation of oil and gas resources requires progressively deeper drilling, deep wells have been one of the important areas in the petroleum-related industry. Due to the complex geological conditions and high rock hardness typical of deep reservoirs, the applicability of conventional mechanical rock breaking technology is becoming progressively limited due to several factors such as low drilling speed, extremely long durations, extensive cut wear, and high costs (Lukawski et al., 2014; Olson and Olson, 1975).

Laser irradiation is a non-contact rock-breaking method that mainly uses a laser beam to radiate the rock surface (Nath, 2014; Pan et al., 2022; Ma et al., 2008). Here, light energy is converted into heat and transferred to the interior of the rock (Xu et al., 2002, 2004b). Owing to the sudden increase in local temperature, the rock breaks under the action of thermal stress (Bybee, 2006). With the increase in the temperature, the rock undergoes a phase change (e.g., fusion and vaporization) (Chen et al., 2019b; Xu et al., 2004b). Thus, rock breakage by laser radiation is expected to emerge as a

* Corresponding author. Hubei Key Laboratory of Waterjet Theory and New Technology, Wuhan University, Wuhan, 430072, Hubei, China.
** Corresponding author.
E-mail addresses: huxiaoyi@whu.edu.cn (Y. Hu), wzf@wust.edu.cn (Z.-F. Wang).

https://doi.org/10.1016/j.petsci.2022.06.008

novel drilling method with considerable application potential (Batarseh et al., 2017), as shown in Fig. 1.

The key to rock breaking by laser irradiation is to control the interaction between the laser and the rock to destroy the largest rock volume with the smallest possible laser energy. This process involves many factors such as the laser parameters, rock properties, and the working state of laser-rock interaction. Thus, rock breakage by laser irradiation has been studied extensively to optimize the rock breaking effect of the laser and to clarify the interaction and breaking mechanism of the laser and the rock (Bharatish et al., 2019; Desai and Shah, 2020; Wang et al., 2019). Gahan and Samih (2001) used an Nd: YAG laser to conduct fixed-point perforation experiments on sandstone, shale, and limestone, and analyzed the effects of laser power, laser frequency, pulse width, and irradiation time on the energy consumption of the rock breaking process by laser irradiation. Xu et al. (2002) examined a 6 kW CO_2 laser to study the beam transmission mode (i.e., continuous wave, normal pulse, and ultra-pulse) and the rock breaking effect of sandstone and limestone under the blowing mode. Erfan et al. (Erfan et al., 2017, 2018) studied the influence of the environment where the laser and rock interact on rock breaking by laser irradiation. Batarseh et al. (2017) investigated the effect of laser irradiation on rock porosity, permeability, and strength. The effect of different parameters on the specific energy of laser drilling was studied by Xu et al. (2003, 2005) through laboratory experiments. Based on these results, a thermal spalling model was established for the specific energy of laser drilling. Ashena and Nabaei (2010) examined the specific energy (SE) of sandstone and limestone under saturated and unsaturated conditions in the laboratory. The results of the study indicated that the higher the core saturation, the higher the SE. The effect of rock-soaking liquids such as water and heavy oil on the SE was explored by Ahmadi et al. (2011, 2012), which assessed the rock breakage by an Nd: YAG laser. From their results, the SE of the samples saturated with water was higher than that of those saturated with heavy oil, and the SE of the samples saturated with heavy oil exceeded that of dry samples.

The heat transfer and exchange in process in laser irradiation can be described as three-dimensional unsteady heat transfer involving heat conduction, convection, and radiation (Collins and Gremaud, 2011). Zhang et al. (2014) simulated the phase transition by using the equivalent specific heat capacity and increasing the aerodynamic source term, and also tracked the mass loss caused by evaporation and boiling at the liquid-gas interface. Ganesh et al. (1997a, 1997b) reported a volume of fluid method for tracking free surfaces to simulate the laser drilling process. Graves and O'Brien (1998) established an energy equation for an infinite sandstone surface with no heat transfer at the boundary. Xu et al. (2004b) developed a numerical procedure to model the entire rock breaking process by laser irradiation. It was found that increasing the relaxation time can effectively prevent the rock melting caused by excessively long irradiation at the same position. Xu et al. (2004a) used FEM to determine rock temperature and calculate the corresponding thermal stress. Agha et al. (2004) conducted a numerical simulation of the transient thermal analysis of limestone and sandstone subjected to laser irradiation. Kasimova and Obnosov (2013) established a heat conduction model by assuming a constant intensity laser beam and a homogeneous elastomer sample. San-Roman-Alerigi and Batarseh (2016) examined the thermo-mechanical coupling physics of laser-rock interaction and studied the heat transfer process during the phase changes in laser drilling using COMSOL Multiphysics. A numerical model of the thermal stresses in granite subjected to laser irradiation was built by Ndeda et al. (2017a, 2017b). As the results indicate, the stress caused by the rise in temperature exceeded the strength of the weakest mineral component, resulting in fracture formation within the rock.

Rock breakage is becoming increasingly challenging in accessing energy resources stored in deep and hard rock formations. Laser irradiation has emerged as a novel drilling method with considerable in this context. Earlier studies mostly focused mostly on examining the effect of laser parameters and rock properties on rock breakage. However, few studies focus on improving the rock breaking effect under the condition that the total energy of laser irradiation remains unchanged. In this study, the number of holes for irradiation and the irradiation power are changed while the total energy of irradiation remains unchanged. The changes in the fracture length, fracture complexity, hole size, and rock breaking efficiency are observed. The results may be applied to evaluate the efficiency of rock breaking under the assistance of laser beams, and may also provide an experimental basis for the practical application of lasers.

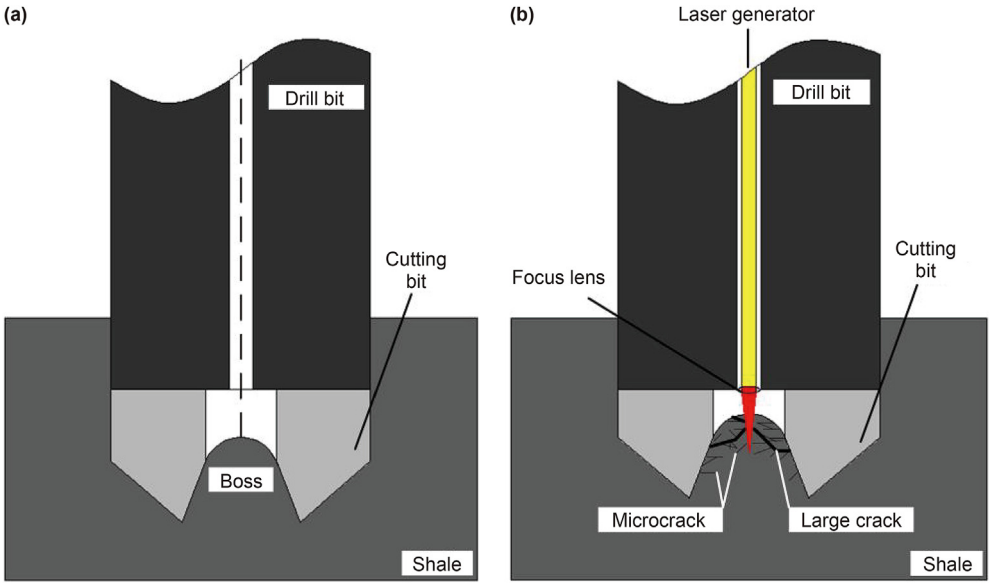

Fig. 1. Schematic diagrams for drilling principle (Lu et al., 2013) (**a**) and laser assist principle (**b**).

2. Experimental

2.1. Experimental setup

The shale samples in this study were irradiated by a fiber laser QCW-150W with a central wavelength of 1080 nm (as shown in Fig. 2). The maximum output power of the laser was 150 W with a power instability of less than 3%. Besides, the fiber core diameter was 50 μm.

2.2. Materials

The samples used in this study were excavated from an outcrop of shale in Changning, Sichuan Province, China. These were shaped into standard samples with dimensions of ϕ50 mm × 100 mm (Fig. 3). All the samples should be heated at 103 °C for 24 h to remove the moisture before being weighed. The physical properties of the shale were obtained by a mechanical testing system. The average uniaxial compressive pressure and tensile strength of the shale specimens are 97.52 MPa and 6.84 MPa, respectively. Other properties such as the density, elastic modulus, and Poisson's ratio are also listed in Table 1. As shown in Table 2, the main components of the shale specimens are SiO_2, CaO, Al_2O_3, MgO, and K_2O.

2.3. Methods

In this experiment, the influence of laser power and the number of irradiation holes on rock breaking is investigated based on the same total energy of laser irradiation. Specimens with one, two, three, and four holes are irradiated with lasers of different powers. As shown in Fig. 4, the distance between the two holes is maintained at 10 mm, and the laser irradiation clockwise depending on the position of the holes. Three sets of experiments are conducted for the same irradiation condition. The details of the experimental scheme in this study are shown in Table 3.

2.4. Thermal breaking theory

The laser power density is the ratio of the laser power to the irradiated area, and the mathematical formula is as follows:

$$F = \frac{4P}{\pi d^2} \tag{1}$$

where F is the laser power density; P is the laser power, W; and d is the diameter of the spot, mm.

The heat conduction equation is expressed in the differential form as (Lehnhoff and Scheller, 1975):

$$q = -k\mathrm{grad}T \tag{2}$$

where q is the heat flux density, W/m^2; k is the thermal conduction coefficient; and T is the temperature field inside the object.

Based on the principle of energy conservation, the sum of the energy generated by the volume element inside the object flowing into its interior through the boundary within unit time is the enthalpy increment, which may be expressed by the Gaussian law as (Siegesmund et al., 2018):

$$\iiint_V \left[\mathrm{div}(k\mathrm{grad}T) + R_V - \frac{\partial}{\partial t}(\rho CT)\mathrm{d}V\right] = 0 \tag{3}$$

where R_V is the power density of the heat source, W/m^3; ρ is the density of rock, kg/m^3; and C is the specific heat of rock, J/(kg K).

The conditions for the equation to be solvable are as follows:

$$\mathrm{div}(k\mathrm{grad}T) + R_V = \frac{\partial}{\partial t}(\rho CT) \tag{4}$$

Converting it to the differential equation of heat conduction in cylindrical coordinates (Wang et al., 2019), the new form is

$$k\left[\frac{1}{r}\frac{\partial}{\partial r}\left(r\frac{\partial T}{\partial r}\right) + \frac{\partial^2 T}{\partial z^2}\right] + \frac{R_V}{k} = \rho C\frac{\partial T}{\partial t} \tag{5}$$

The thermo-mechanical coupling equation can be written as (Siegesmund et al., 2018):

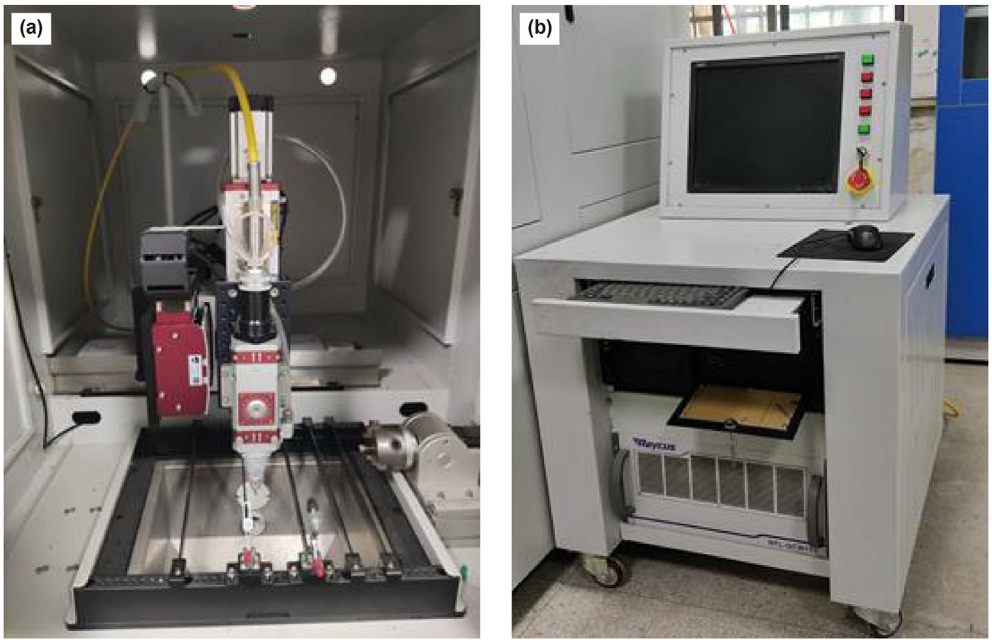

Fig. 2. (**a**) Laser irradiation set-up and (**b**) computer device.

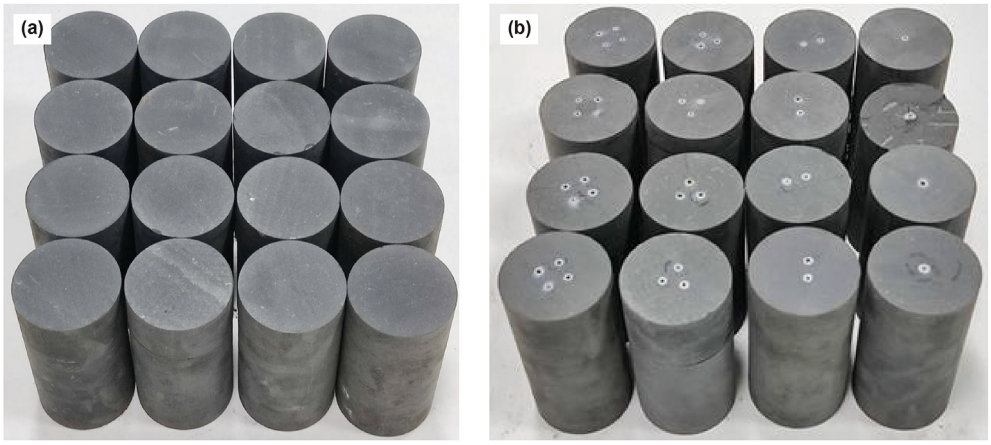

Fig. 3. Shale specimens before (**a**) and after (**b**) the experiment.

Table 1
Physical properties of shale.

Density, g/cm^3	Elastic modulus, GPa	Poisson's ratio	Uniaxial compressive pressure, MPa	Tensile strength, MPa
2.56	12.35	0.32	97.52	6.84

$$kT_{ii} + Q = \rho C\dot{T} + \beta T_0 \dot{\varepsilon_{kk}} \tag{6}$$

where Q is the generation rate of heat; β is the thermal stress coefficient; T_0 is the initial temperature; and ε_{kk} is the strain.

When the sample is heated by the laser, both tensile and compressive stresses will be generated inside the unit. The magnitudes of these two forces determine whether the unit deforms. The damage to the element due to thermal stress is represented by D. When the unit is subjected to tensile stress, it can be expressed as (Li and Huang, 2017; Pan et al., 2021):

Table 2
Chemical composition of shale.

Mineral	SiO_2	CaO	Al_2O_3	Fe_2O_3	MgO	K_2O	Others
Mass fraction, %	72.5	4.56	10.68	4.66	1.88	1.08	4.64

$$D = \begin{cases} 0 & (\varepsilon < \varepsilon_{t0}) \\ 1 - \dfrac{\sigma_{tr}}{\varepsilon E_0} & (\varepsilon_{t0} \le \varepsilon \le \varepsilon_{tu}) \\ 1 & (\varepsilon > \varepsilon_{tu}) \end{cases} \tag{7}$$

where σ_{tr} is the tensile damage residual strength; ε_{t0} is the elastic limit of tensile strain; ε_{tu} is the maximum tensile strain; E_0 is the initial elasticity modulus. When $\varepsilon < \varepsilon_{t0}$, the crystal units are not broken, and the rock is not deformed. When $\varepsilon_{t0} \le \varepsilon \le \varepsilon_{tu}$, the crystal unit is in the elastic deformation zone, and the rock is in a critical state where it is about to fragment. When the condition $\varepsilon > \varepsilon_{tu}$ is met, the crystal units are destroyed and the rock is deformed, resulting in rock fragmentation.

Therefore, the thermal stress based on the temperature difference may be denoted as (Pan et al., 2022):

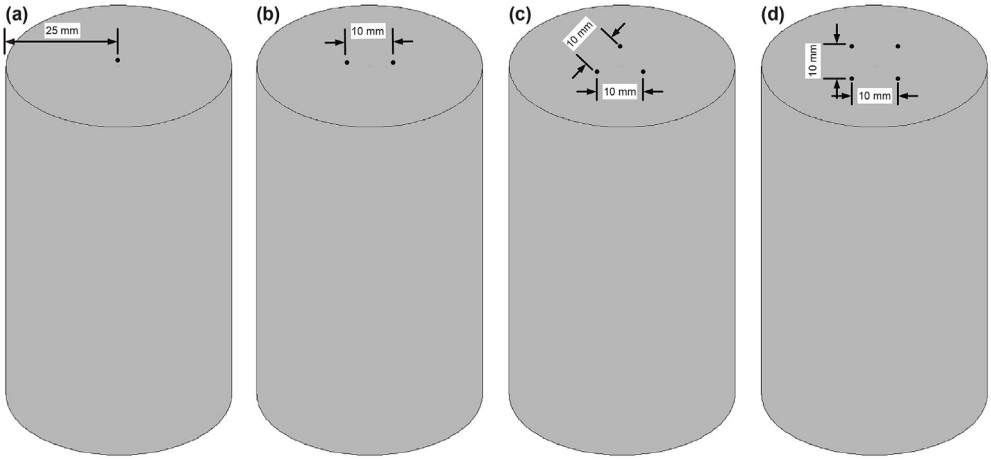

Fig. 4. Schematic diagrams of specimens with different number of irradiation holes: (**a**) single hole, (**b**) double holes, (**c**) three holes, (**d**) four holes.

Table 3
Experimental scheme for laser irradiation.

Laser power, W	Specimen	Number of holes	Irradiation time, s
90	#1	1	108
	#2	2	54
	#3	3	36
	#4	4	27
116	#5	1	84
	#6	2	42
	#7	3	28
	#8	4	21
135	#9	1	72
	#10	2	36
	#11	3	24
	#12	4	18

$$\sigma_{ij}=\begin{cases}\lambda\varepsilon_{kk}\delta_{ij}+2G\varepsilon_{ij}-\beta\Delta T\delta_{ij} & (\varepsilon<\varepsilon_{t0})\\ \dfrac{\sigma_{tr}}{\varepsilon E_0}\left(\lambda\varepsilon_{kk}\delta_{ij}+2G\varepsilon_{ij}-\beta\Delta T\delta_{ij}\right) & (\varepsilon_{t0}\le\varepsilon\le\varepsilon_{tu})\\ 0 & (\varepsilon>\varepsilon_{tu})\end{cases} \tag{8}$$

where G is the shear modulus; δ_{ij} is the Kronecker function.

When the thermal stress field created by the laser exceeds the condition stipulated for rock fracture, fractures may be generated on the rock surface. Hence, the rock can be broken by physical methods to remove it.

3. Results

In this study, the effects of laser power and the number of irradiation holes on rock breaking by laser irradiation are examined by controlling the total energy of the laser irradiation. The electronic image method is used to extract and quantitatively analyze the fracture region (Chen et al., 2019a).

3.1. Observation of macrofracture after laser irradiation

Fracture tortuosity (FT) is an important means to characterize the macroscopic complexity of the fracture (Liu et al., 2019; Zhao et al., 2018), and it can be expressed as:

$$\tau_f=\frac{L_f}{L_d} \tag{9}$$

where τ_f is the fracture tortuosity, a dimensionless parameter; L_f denotes the bending length of the fracture obtained in the picture; and L_d denotes the straight-line distance of the fracture endpoint in the picture.

In this study, the rock surface is analyzed quantitatively by combining photoshop and an electronic image method to extract and quantify the fracture length. Fig. 5(a) and (b) show the rock surfaces of the shale and the extracted fracture images, respectively. Jia et al. (2018) used the same method to investigate the fracture tortuosity, which can be expressed as:

$$\tau_f=\sum_{i=1}^{n}L_{fi}\Big/\sum_{j=1}^{n}L_{dj} \tag{10}$$

where $\sum_{i=1}^{n}L_{fi}$ is the actual fracture length of the shale surface and $\sum_{j=1}^{n}L_{dj}$ is the total straight-line distance until the endpoint of the fracture in the picture.

3.1.1. Impact of number of irradiation holes on fracture morphology

Fig. 6 shows the shale morphology after irradiation with a different number of irradiation holes for a laser power of 90 W. The fractures appear near the hole and the fractures are directed extends towards the edge of the shale, as shown in Fig. 6(a). This is because the thermal stress produced by laser drilling is concentrated in the vicinity of the hole, resulting in macroscopic fractures. Fig. 6(b) shows double-hole irradiation with a spacing of 10 mm between the two holes. Each of the two holes produces the main fracture, that extends from the periphery of the hole to the edge of the sample surface. The thermal stress produced by the laser drilling causes the formation of fractures that connect the two holes. Fig. 6(c) shows three-hole irradiation. It can be seen that the fracture network is more complicated than in the case of single- and double-hole irradiation. Each hole has a main fracture, in addition to a connection fracture between the No. 2 and No. 3 holes. Fig. 6(d) shows the four-hole irradiation effects. With the increase in the number of holes, the irradiation time per hole and the fracture density on the surface of the shale decrease. There are no major penetrating major fractures on the shale surface and no connecting fractures between the holes. Only small fractures are generated around the No. 3 and No. 4 holes. This is because the more the holes are irradiated by low power, the more the energy dissipated. The energy absorbed by the sample is not sufficient to quickly break the rock and expand the fracture.

Fig. 7 shows the shale morphology after irradiation with different numbers of irradiation holes at the laser power of 116 W. The main fracture extends to the edge of the rock, and branch fractures are generated around the hole, as shown in Fig. 7(a). Fig. 7(b) shows double-hole irradiation. Each of the two holes produces the main fracture, and another fracture is generated that connects the holes. There is a bifurcation fracture on one side of the main fracture of the No. 2 hole. Fig. 7(c) shows the three-hole specimen subjected to irradiation. The No. 1 and No. 2 holes have one main fracture associated with them, respectively. The No. 3 hole is associated with two main fractures. The No. 1 and No. 3 holes have connection fractures, and several branch fractures are generated. Fig. 7(d) depicts the four-hole irradiation. The No. 1 and No. 2 holes each have one main fracture, respectively. The main fracture generated by the No. 3 hole changes direction. It can be seen that more small fractures and branched fractures are produced by the four-hole irradiation process than by the single-hole irradiation, double-hole irradiation, or three-hole irradiation processes. With the increase in the number of holes for irradiation, the heat dissipated from the center of the rock to the surroundings increases, while the heat-affected area increases, which is conducive to the generation of more branch fractures.

Fig. 8 shows the shale morphology after irradiation with different numbers of irradiation holes at a laser power of 135 W. For the single-hole sample, three main fractures are generated around the hole and these gradually extend to the edge, as shown in Fig. 8(a). Fig. 8(b) shows the irradiation of the double-hole specimen. The No. 1 hole has a main fracture that extends to the edge of the rock. Three main fractures surround the No. 2 hole. In addition, there is a fracture that connects the two holes, as well as several smaller fractures on the surface of the shale. Fig. 8(c) shows the irradiation of the three-hole sample. There are many small fractures around the No. 1 hole. The main fracture changes direction as it approaches the No. 1 hole and connects with the No. 3 hole. Another main fracture extends from the edge of the specimen to the inside, with two branches reaching to the No.1 hole and No.3 hole, respectively. The main fracture that is generated by the No. 2 hole is annular and extends to the edge of the rock. Besides, the three holes are connected. Fig. 8(d) shows the irradiation of a three-hole specimen. Fractures on the shale surface increase with the

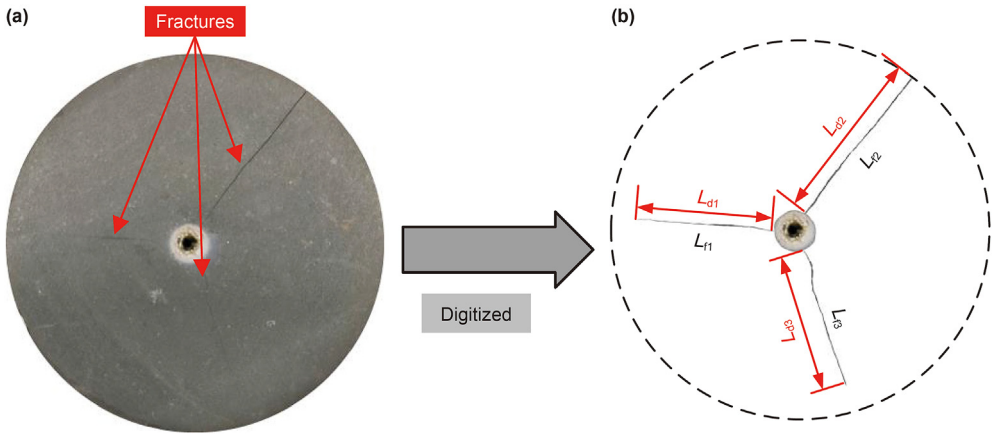

Fig. 5. Schematic of fracture tortuosity: (**a**) appearance of the shale surface, (**b**) extracted fractures.

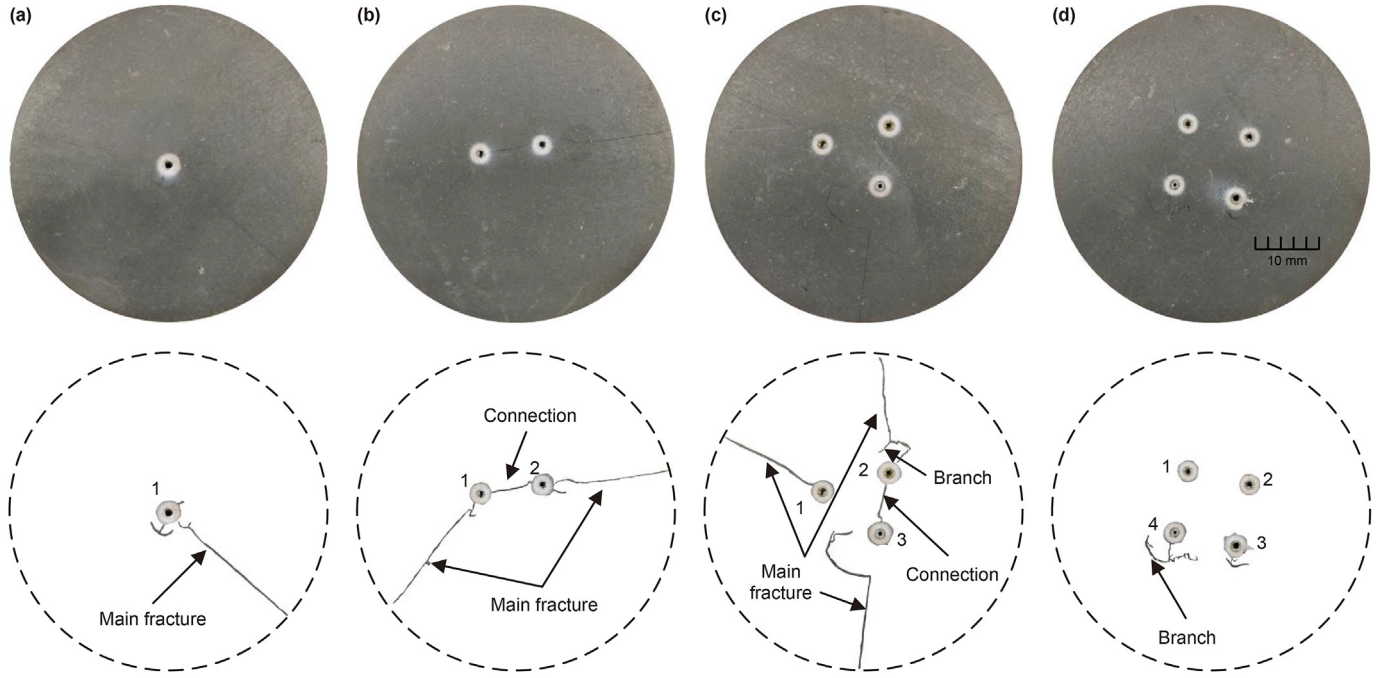

Fig. 6. Surface appearance (upper) and fracture (lower) of shales with different numbers of holes at a laser power of 90 W: (**a**) single-hole specimen, (**b**) double-hole specimen, (**c**) three-hole specimen, (**d**) four-hole specimen.

increase in the number of holes. Each of the four holes has a main fracture, and the connection and crossover between the fractures become more obvious during expansion.

3.1.2. Impact of power on fracture morphology

Fig. 9 shows the variation of the fracture length and tortuosity under different intensities of laser power. The changes in fracture length and tortuosity for a 90 W laser power are shown in Fig. 9(a). With the increase in the number of irradiation holes, the fracture length of the shale irradiated by the laser increases from 3.04 to 7.56 cm and then decreases to 1.7 cm, while the fracture tortuosity increases from 1.05 to 1.26 and then decreases to 1.14. The fracture length and tortuosity are the largest when there are three irradiation holes. When the laser power is 90 W, the energy dissipated during the irradiation of the four-hole specimen is more, and the energy absorbed by the sample is not sufficient to cause more fractures in the rock. The changes in the fracture length and tortuosity at the laser power of 116 W are shown in Fig. 9(b). With the increase in the number of irradiation holes, the fracture lengths are 4.30, 5.93, 12.19, and 11.16 cm, respectively, and the fracture tortuosity shows a direct increase. The heat dissipation from the center of the rock and the heat-affected zone also increase, which promotes the formation of branch fractures and increases the fracture tortuosity. The changes in fracture length and tortuosity corresponding to a laser power of 135 W are shown in Fig. 9(c). This shows that increasing the number of irradiation holes is more conducive to fracture propagation and tortuosity under high laser power irradiation.

Figs. 6(a), 7(a) and 8(a) are the morphologies of the specimens after the irradiation of the single-hole specimens at 90, 116, and 135 W, respectively. A single main fracture and very few branch fractures are created around the hole corresponding to the laser power of 90 W. When the laser power is increased to 116 W, there is only one main fracture, however, a long and curved branch fracture

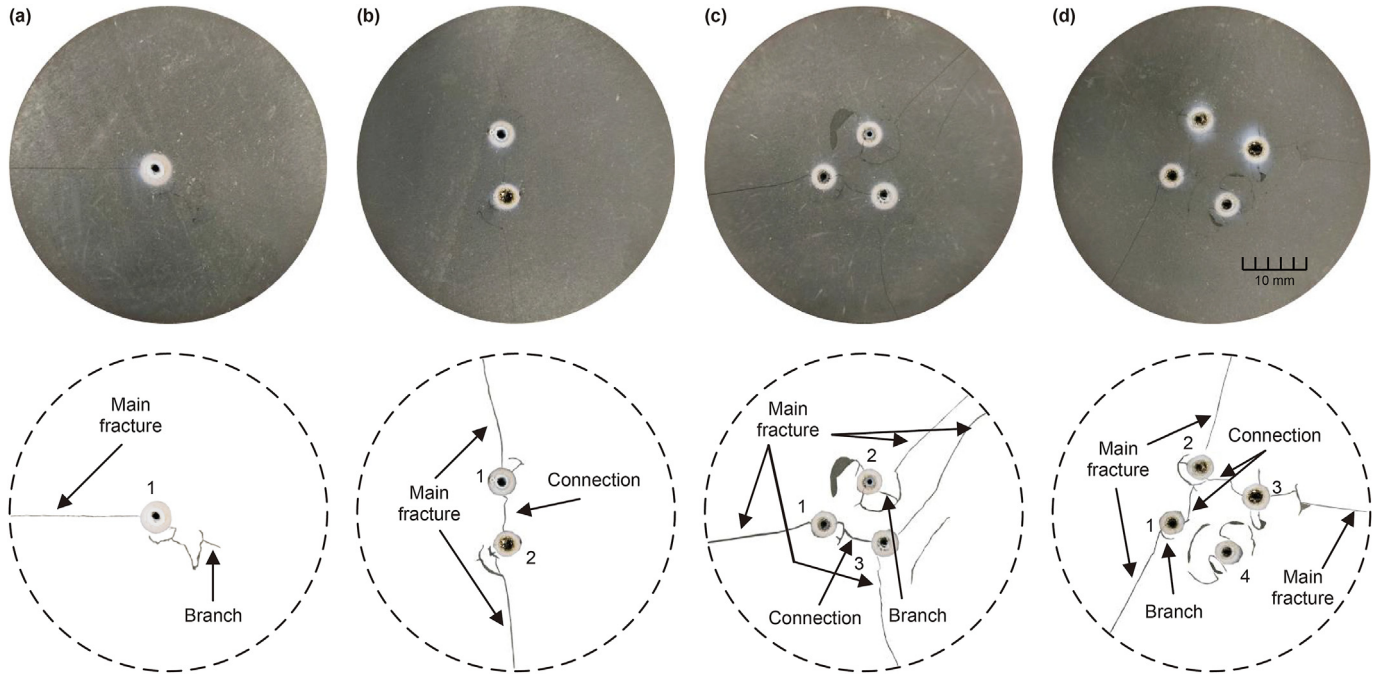

Fig. 7. Surface appearance (upper) and fracture (lower) of shales with different numbers of holes at a laser power of 116 W: (**a**) single-hole specimen, (**b**) double-hole specimen, (**c**) three-hole specimen, (**d**) four-hole specimen.

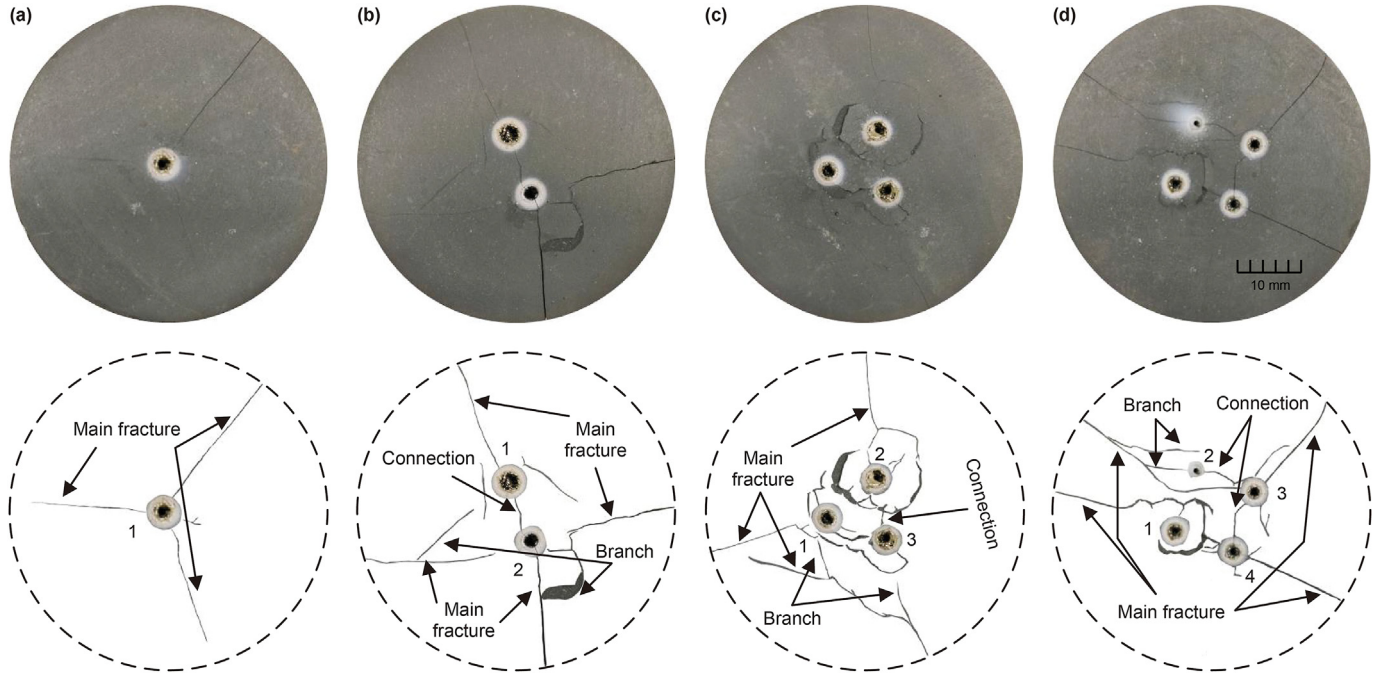

Fig. 8. Surface appearance (upper) and fracture (lower) of shales with different numbers of holes at a laser power of 135 W. (**a**) Single-hole specimen, (**b**) double-hole specimen, (**c**) three-hole specimen, (**d**) the four-hole specimen.

is generated. Three main fractures are generated in the vicinity of the hole as the laser power is increased to 135 W. With the increase in the laser power, the fracture length of the laser-irradiated increases from 3.04 to 6.31 cm. Figs. 6(b), 7(b) and 8(b) are the morphologies of the specimens after the irradiation of the double-hole specimen at 90, 116, and 135 W, respectively. The images show two main fractures generated and the two holes being connected by a fracture under the laser power of 90 W. Branch fractures are generated around the two holes when subjected to a laser power of 116 W. When the laser power is 135 W, four main fractures form around the hole along with a greater number of branch fractures. With the increase in the laser power, the fracture length of the shale irradiated by laser increases from 4.93 to 12.96 cm. Figs. 6(c), 7(c) and 8(c) are the morphologies of the specimens after the irradiation of the three-hole specimen at 90, 116, and 135 W, respectively. There are three main fractures and the two holes are connected by

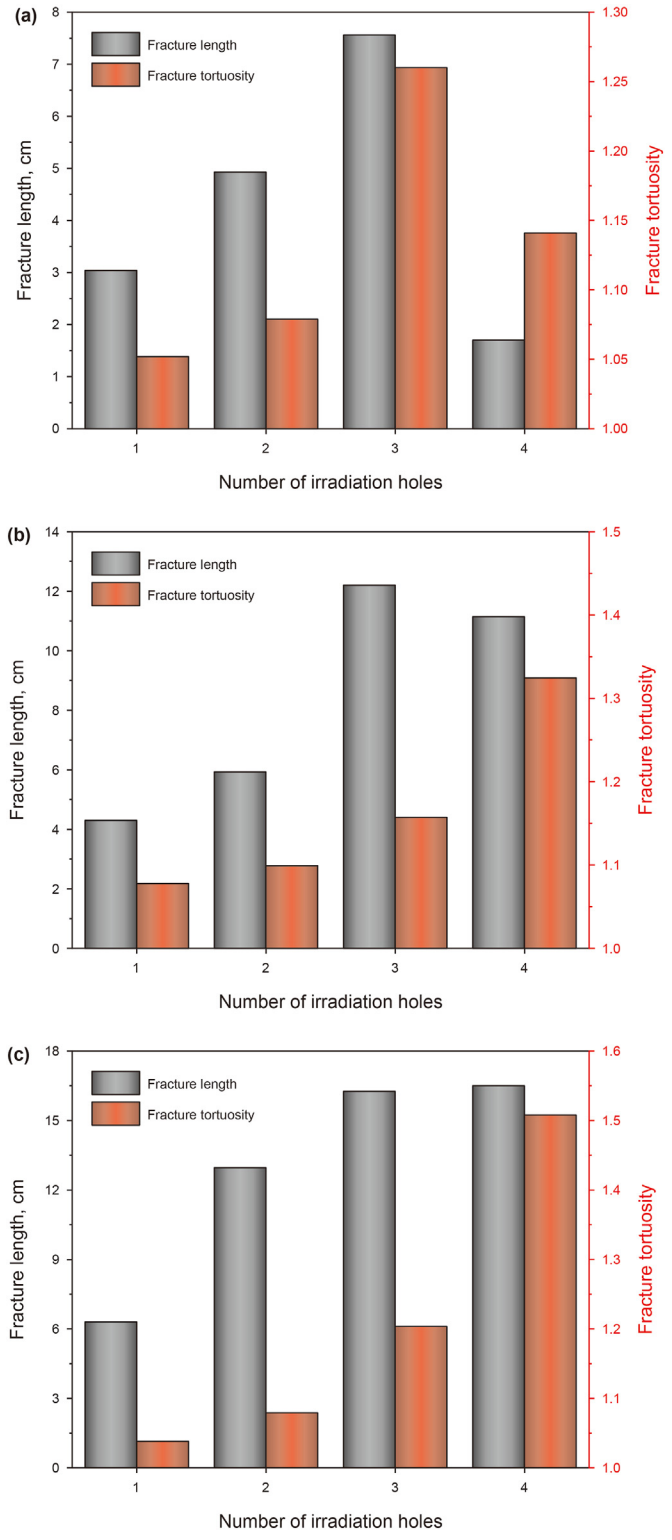

Fig. 9. Fracture length and fracture tortuosity versus the number of irradiation holes under different laser power: (**a**) 90 W, (**b**) 116 W, (**c**) 135 W.

these fractures when subjected to a 90 W laser. When the power is increased to 116 W, four main fractures are generated around the irradiation holes. The number of branch fractures shows an obvious increase and spalling occurs on the rock surface. When the laser power is 135 W, the main fractures develop branches, and the area of rock surface susceptible to spalling increases. With the increase in the power of the laser, it can be observed that the fracture length of shale irradiated by the laser increases from 7.56 to 16.26 cm. Figs. 6(d), 7(d) and 8(d) show the morphologies of the specimens after the irradiation of the four-hole specimen at 90, 116, and 135 W, respectively. Relatively fewer fractures are generated around the No. 3 and No. 4 holes under the laser power of 90 W. When the laser power becomes 116 W, two main fractures form, while the number of branch fractures increases. Moreover, there will form main fractures, and as a result, the holes become closely connected when the laser power is further increased to 135 W. The increase in the laser power is accompanied by an increase in the fracture length of shale irradiated by laser from 1.7 to 16.51 cm. Predictably, when the area of laser irradiation remains the same, as the laser power is increased, the laser intensity also increases. Therefore, the greater the laser energy absorbed by a rock per unit time, the more conducive it will become to fracture propagation and subsequent fracture fragmentation.

3.2. Analysis of hole size

In summary, on the whole, mass removal in the samples was accomplished by melting and evaporation (Zhang et al., 2016). The hole depth was increased primarily by evaporation, while the increase in the hole diameter was largely owing to the melting of the rock. Subsequently, the molten material was eliminated primarily by the residual steam force.

Fig. 10(a) shows the variation in the hole diameter with the increase in laser power. As the laser power increases, the hole diameter also increases gradually. The change in the number of holes does not affect the hole diameter considerably under constant power. Meanwhile, the hole diameter ranges corresponding to 90, 116, and 135 W laser powers are 1.07–1.36, 1.68–1.89, and 2.08–2.56 mm, respectively. It can be seen from Eq. (1) that the more powerful the laser is, the stronger the laser intensity will be when the laser irradiation area remains constant. Therefore, it is more conducive to the increase in the hole diameter. Fig. 10(b) shows the variation in the depth of the single hole with the increase in laser power. When the number of irradiation holes is the same, the hole depth increases with the increase in the laser power. This is because, with a higher power, the single-hole laser intensity also increases, resulting in a larger residual vapor force. This helps to remove the rock and increase the hole depth. For the same laser power, the depth of each hole decreases with the increase in the number of holes.

Fig. 11 shows the relationship between the hole depth and the irradiation time under different laser power. The laser power exerts a fierce impact on the hole depth under constant laser energy. Meanwhile, as the number of irradiation holes increases, the hole depth is reduced by about 3/4, 2/5, and 3/10 at 90, 116, and 135 W, respectively. This is because the total output energy of each sample is the same. Increasing the number of holes will reduce the irradiation time for a single hole, leading to a decrease in the absorbed energy that is not conducive to the increase in the hole depth. This indicates that the hole depth of the sample aggravates with the increase in the irradiation time of a single hole. The relationship between the hole depth (h) and the irradiation time (t) of the sample follows a polynomial function:

$$h = A + Bt + Ct^2 \tag{11}$$

where A, B, and C are the regression coefficients. It can be seen from Fig. 11 that all the determination coefficients (R^2) of the fitted curves exceed 0.95.

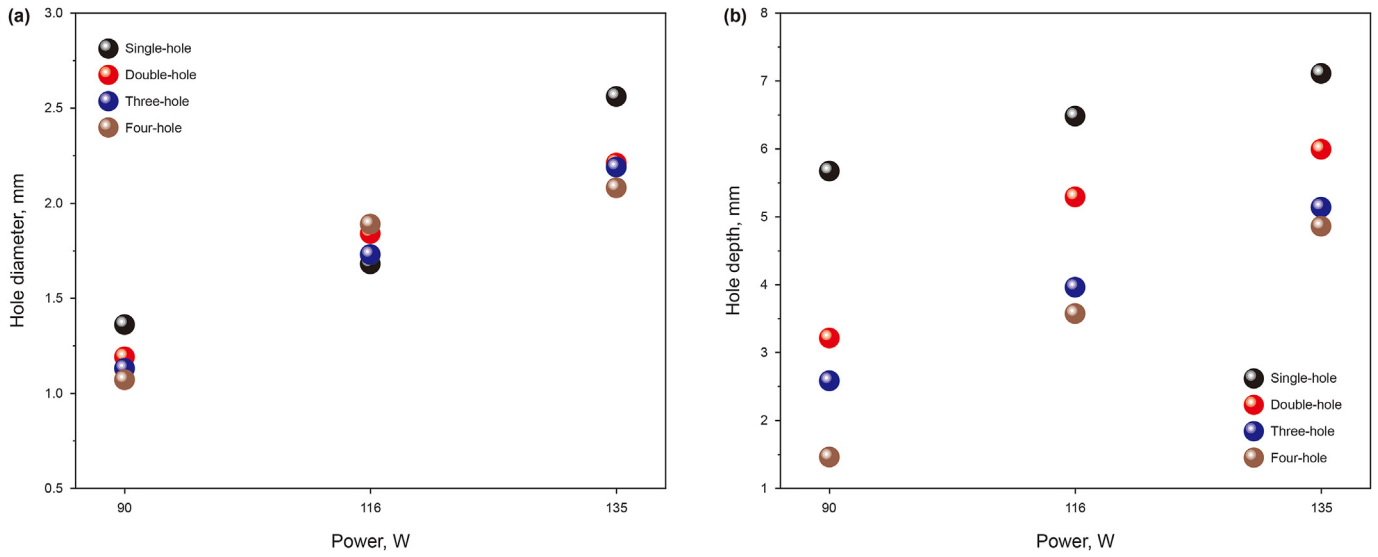

Fig. 10. Plots of the hole diameter (**a**) and hole depth (**b**) versus the laser power.

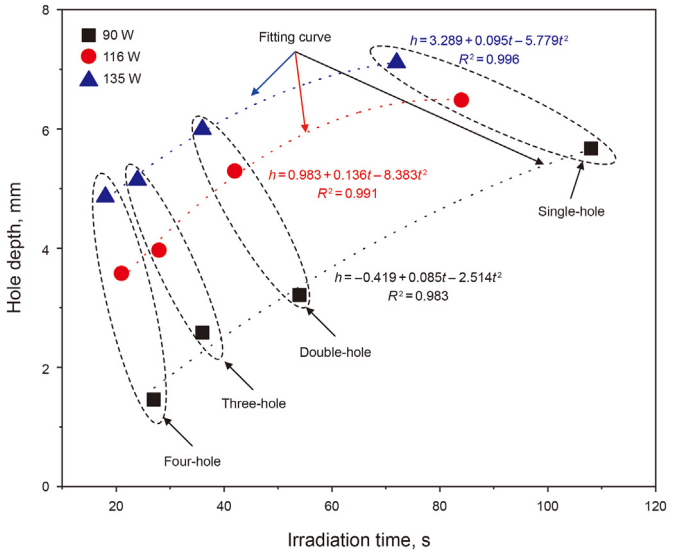

Fig. 11. Relationship between the hole depth and the irradiation time under different laser power.

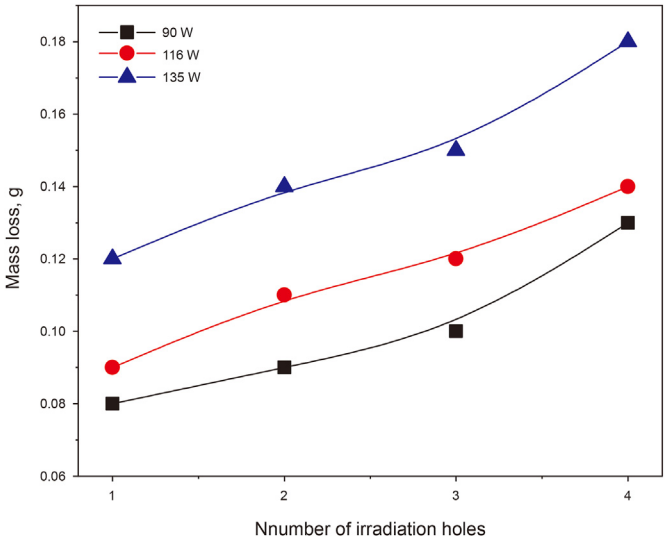

Fig. 12. Effect of the number of irradiation holes on mass loss of rock.

3.3. Efficiencies of laser irradiation in rock breaking

The hole formation and mass loss were attributed to the melting and evaporation of the surface of the shale sample irradiated by laser. Thus, the breakage of the shale sample should be analyzed using evaluation indexes.

3.3.1. Mass of removed sample

Fig. 12 shows the variation of the removed mass with laser power for a different number of holes. As the number of holes increases, the mass loss also increases gradually under different values of laser power. The mass loss of rock with the laser power of 90, 116, and 135 W increases from 0.08, 0.09, and 0.12 g to 0.13, 0.14, and 0.18 g, respectively. This is because the irradiated area of the rock increases gradually with the increase in the number of the holes, resulting in the removal of a greater mass of rock. When the number of irradiation holes is the same, the mass loss of the rock increases with the increase in the laser power. When the total output energy of the laser is the same for all the cases, the greater the power, the shorter the laser irradiation time. Consequently, the lesser the energy dissipation, the more favorable the conditions are for rock to be melted and evaporated by the high temperature.

3.3.2. Specific energy and modified specific energy

The shale specimen density is indicated by:

$$\rho = \frac{m}{\pi R^2 h} \tag{12}$$

where ρ is the density of the shale, g/cm^3; m is the mass of the shale specimen, g; and R and h are the radius and height of the specimen, respectively, cm.

The hole and mass loss were attributed to the melting and evaporation of the shale sample surface irradiated by laser. Thus, the breakage of the shale sample should be analyzed by the evaluation indexes. Specific energy (SE) represents the energy required

to remove a unit volume of rock (Ahmadi et al., 2011). The specific energy may be represented by:

$$E_s = \frac{P*t}{V_R} \tag{13}$$

where E_s is the specific energy, kJ/cm^3; P denotes the laser power, W; t is the time of laser irradiation, s; and V_R is the volume of the shale sample removed by the laser radiation, cm^3.

However, the volume of rock removed by the same laser differed from sample to sample owing to the heterogeneity of rock. Accordingly, the modified specific energy (MSE) is defined as the energy required per unit mass of the rock sample. The formula for the MSE is given by (Pan et al., 2022):

$$E_m = \frac{P*t}{M_R} \tag{14}$$

where E_m is the modified specific energy; M_R represents the mass of the shale sample removed by the laser irradiation.

Based on Eqs. (13) and (14), respectively, the variations of the SE and MSE of the laser-irradiated shale samples under different laser power are plotted in Fig. 13. Fig. 13(a) shows that the SE and MSE decrease with the increase in the number of holes under a laser power of 90 W. The SE decreases from 345.5 to 165.9 kJ/cm^3 and the MSE decreases from 142.9 to 70.8 kJ/g with the increase in the number of the holes. Fig. 13(b) shows the changes in the SE and the MSE under a laser power of 116 W. The SE decreases from 266.5 to 150.7 kJ/cm^3 while the MSE decreases from 108.1 to 67.4 kJ/g with the increase in the number of holes. Fig. 13(c) shows the changes in the SE and MSE under the laser power of 135 W. The SE decreases from 207.4 to 133.2 kJ/cm^3 and the MSE decreases from 81.3 to 54.1 kJ/g with the increase in the number of holes. As indicated by the results, as the number of the holes increases, the heat required to evaporate the same amount of rock decreases. Meanwhile, the SE and MSE decrease with increasing laser power for the same number of irradiation holes. Thus, increasing the number of irradiation holes and laser power could be beneficial to the efficiency of rock breaking.

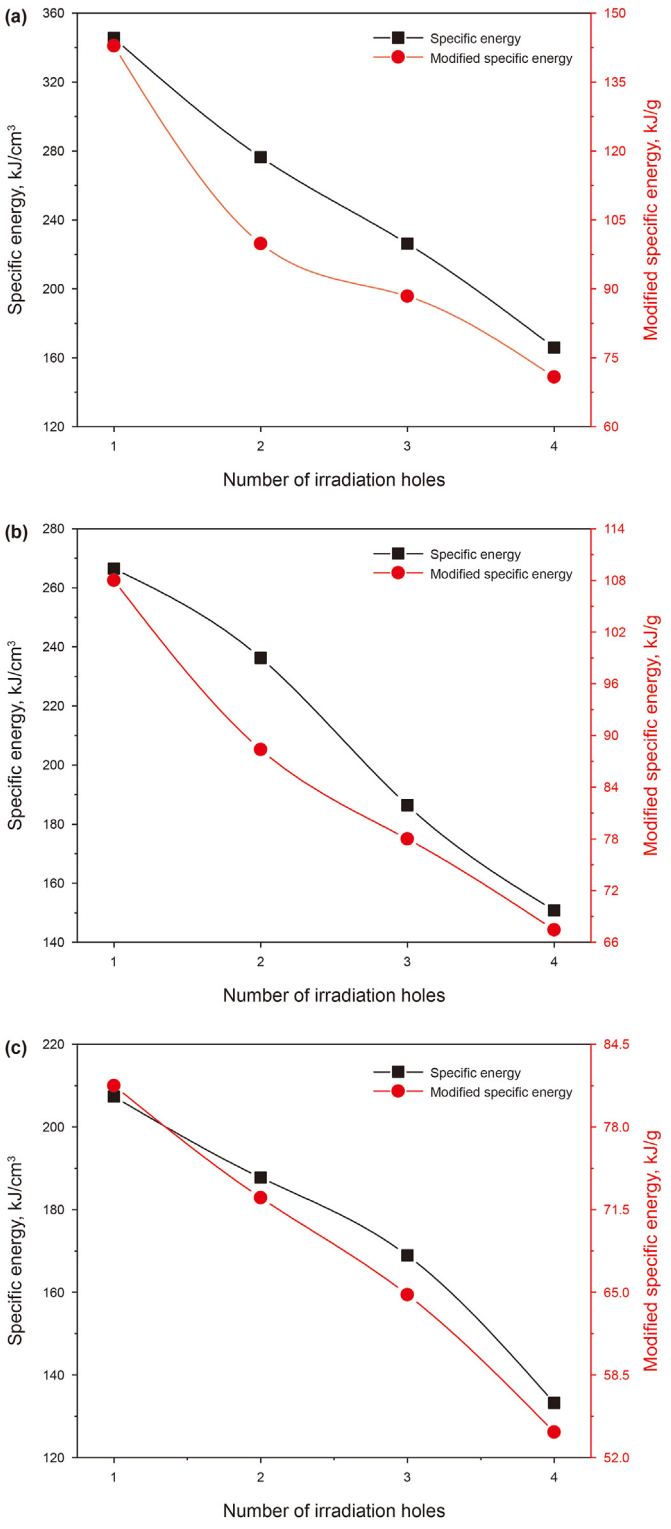

Fig. 13. Specific energy and modified specific energy versus the number of irradiation holes under different laser power: (**a**) 90 W, (**b**) 116 W, (**c**) 135 W.

4. Discussion

In general, rock is an aggregation of a large number of mineral particles. The rock can absorb the laser energy and act on these mineral particles in the form of heat. The heat received by each particle is a function of the position of the particles relative to the spot where the laser hits the rock. The closer the particles are to the center of the laser spot, the higher the heat. The mineral particles undergo thermal expansion after heating, and the thermal expansion among adjacent particles is uneven due to the differences in the heat obtained. This results in tensile and compressive forces between adjacent particles as a pair of the applied and reaction forces, and this constitutes thermal stress. The mineral particles sustain damage when the thermal stress exceeds the stress limit threshold of the mineral particles. With the gradual aggravation of damage, the microcracks expand until macroscopic fractures are formed.

Laser intensity represents the power per unit area and is a measure of the effect of laser power. The laser irradiation time determines the time for the accumulation of laser energy on the rock surface. When the laser intensity is low and not enough to break the rock quickly, the laser irradiation time may be increased to achieve rock fragmentation. For example, the four-hole irradiation with a power of 90 W, which is relatively low in power and high in energy dissipation, is not conducive to the generation and expansion of rock fractures. On the contrary, when a high laser power (e. g., 116 and 135 W) irradiates the rock, there is less dissipated energy and thus, increasing the number of irradiation holes is conducive to the generation and expansion of fractures in the rock. In addition, increasing the number of irradiation holes is beneficial to increasing the irradiation area, improving energy

utilization, increasing the mass loss of rock, and reducing SE and MSE.

5. Conclusions

In this study, the effects of the number of irradiation holes and laser power on the rock fracture length, fracture tortuosity, hole size, and rock breaking efficiency are studied under the condition of constant total irradiation energy of the laser. The following conclusions can be drawn:

(1) Increasing the power causes the laser intensity to increase which is more conducive to the formation of larger and deeper holes, based on the constant total energy of laser irradiation. The range of hole diameter increases from 1.07–1.36 to 2.08–2.56 mm. Under the condition of constant laser power, more holes help reduce the energy absorbed by each hole. The hole depth is reduced by about 3/4, 2/5, and 3/10 at 90, 116, and 135 W, respectively.

(2) When the total energy of the laser irradiation is constant, the fracture length and fracture tortuosity of the rock irradiated by the low laser power will first increase and then decrease with the increase in the number of holes, and reach the peak value when there are three irradiation holes. The fracture length and tortuosity of the rock irradiated by the high laser power will increase with the increase in the number of holes. This is because the energy dissipated is more in the low-power irradiation of rock, and the energy absorbed by the sample is not enough to break the rock quickly to expand the fracture.

(3) Increasing the number of holes is beneficial to the mass loss of the rock under constant laser energy. The specific energy (SE) and modified specific energy (MSE) decrease gradually as the number of irradiation holes increases. When the number of irradiation holes is the same, the mass of the shale sample removed by the low laser power is less than that removed by high power, and SE and MSE under low power are greater than those under high power. Thus, a high laser power with multiple holes offers better rock-breaking performance.

Acknowledgements

This work is supported by the National Natural Science Foundation of China (No. 52174004 and No. 51804318), and the National Key Research and Development Program of China (No. 2018YFC0808401).

References

Agha, K.R., Belhaj, H.A., Mustafiz, S., et al., 2004. Numerical investigation of the prospects of high energy laser in drilling oil and gas wells. Petrol. Sci. Technol. 22 (9–10), 1173–1186. https://doi.org/10.1081/LFT-200034061.

Ahmadi, M., Erfan, M.R., Torkamany, M.J., et al., 2011. The effect of interaction time and saturation of rock on specific energy in ND:YAG laser perforating. Opt Laser. Technol. 43 (1), 226–231. https://doi.org/10.1016/j.optlastec.2011.05.017.

Ahmadi, M., Erfan, M.R., Torkamany, M.J., et al., 2012. The effect of confining pressure on specific energy in Nd:YAG laser perforating of rock. Opt Laser. Technol. 44 (1), 57–62. https://doi.org/10.1016/j.optlastec.2011.05.017.

Ashena, R., Nabaei, M., 2010. Experimental investigation of specific energy of rocks by low power laser drilling. Nigeria Ann. Int. Conf. Exhib. https://doi.org/10.2118/136986-MS.

Batarseh, S.I., Graves, R., Obaid, O.A., et al., 2017. High power laser technology in downhole applications, reshaping the industry. In: Abu Dhabi International Petroleum Exhibition & Conference. https://doi.org/10.2118/188507-MS.

Bharatish, A., Kishore Kumar, B., Rajath, R., et al., 2019. Investigation of effect of CO_2 laser parameters on drilling characteristics of rocks encountered during mining. J. King Saud Univ. Eng. Sci. 31 (4), 395–401. https://doi.org/10.1016/j.jksues.2017.12.003.

Bybee, K., 2006. Modeling laser-spallation rock drilling. J. Petrol. Technol. 58 (2), 62–64. https://doi.org/10.2118/0206-0062-JPT.

Chen, H., Hu, Y., Kang, Y., et al., 2019a. Fracture initiation and propagation under different perforation orientation angles in supercritical CO_2 fracturing. J. Petrol. Sci. Eng. 183 (7), 106403. https://doi.org/10.1016/j.petrol.2019.106403.

Chen, Y., Li, S., Qu, X., et al., 2019b. Numerical investigation of growth model for laser-induced damage in optics under high power laser irradiation. Optik 194, 163053. https://doi.org/10.1016/j.ijleo.2019.163053.

Collins, J., Gremaud, P., 2011. A simple model for laser drilling. Math. Comput. Simulat. 81 (8), 1541–1552. https://doi.org/10.1016/j.matcom.2010.07.010.

Desai, J., Shah, V., 2020. Feasibility study and application of iot based hybrid LASER drilling system in geothermal fields. In: 45th Workshop on Geothermal Reservoir Engineering.

Erfan, M.R., Shahriar, K., Sharifzadeh, M., et al., 2017. Moving perforation of rocks using long pulse Nd:YAG laser. Opt Laser. Eng. 94, 12–16. https://doi.org/10.1016/j.optlaseng.2017.02.010.

Erfan, M.R., Shahriar, K., Sharifzadeh, M., et al., 2018. Coupled T-H-M processes' effect on specific energy in continuous wave fiber laser rock perforation. J. Laser Appl. 30 (3), 032005. https://doi.org/10.2351/1.5018799.

Gahan, B.C., Samih, B., 2001. Laser drilling: determination of energy required to remove rock. In: SPE Annual Technical Conference and Exhibition. https://doi.org/10.2118/71466-MS.

Ganesh, R.K., Faghri, A., Hahn, Y., 1997a. A generalized thermal modeling for laser drilling process–II. Numerical simulation and results. Int. J. Heat Mass Tran. 40 (14), 3361–3373. https://doi.org/10.1016/S0017-9310(96)00369-9.

Ganesh, R.K., Faghri, A., Hahn, Y., 1997b. A generalized thermal modeling for laser drilling process—I. Mathematical modeling and numerical methodology. Int. J. Heat Mass Tran. 40 (14), 3351–3360. https://doi.org/10.1016/S0017-9310(96)00368-7.

Graves, R.M., O'Brien, D.G., 1998. StarWars laser technology applied to drilling and completing gas wells. In: SPE Annual Technical Conference and Exhibition. https://doi.org/10.2118/49259-MS.

Jia, Y., Lu, Y., Elsworth, D., et al., 2018. Surface characteristics and permeability enhancement of shale fractures due to water and supercritical carbon dioxide fracturing. J. Petrol. Sci. Eng. 165, 284–297. https://doi.org/10.1016/j.petrol.2018.02.018.

Kasimova, R.G., Obnosov, Y.V., 2013. Topology of steady heat conduction in a solid slab subject to a nonuniform boundary condition: the Carslaw–Jaeger solution revisited. ANZIAM J. 53 (4), 308–320. https://doi.org/10.1017/S1446181112000260.

Lehnhoff, T.F., Scheller, J.D., 1975. The influence of temperature dependent properties of thermal rock fragmentation. Int. J. Rock Mech. Min. Sci. Geomech. Abstracts 12 (8), 255–260. https://doi.org/10.1016/0148-9062(75)91405-9.

Li, Z., Li, L., Huang, B., et al., 2017. Numerical investigation on the propagation behavior of hydraulic fractures in shale reservoir based on the DIP technique. J. Petrol. Sci. Eng. 154, 302–314. https://doi.org/10.1016/j.petrol.2017.04.034.

Liu, J., Hu, Y., Kang, Y., et al., 2019. Experimental study on fracture propagation induced by supercritical CO_2 jet fracturing in artificial samples with prefabricated bedding planes. J. Nat. Gas Sci. Eng. 72, 103037. https://doi.org/10.1016/j.jngse.2019.103037.

Lu, Y., Tang, J., Ge, Z., et al., 2013. Hard rock drilling technique with abrasive water jet assistance. Int. J. Rock Mech. Min. Sci. 60, 47–56. https://doi.org/10.1016/j.ijrmms.2012.12.021.

Lukawski, M.Z., Anderson, B.J., Augustine, C., et al., 2014. Cost analysis of oil, gas, and geothermal well drilling. J. Petrol. Sci. Eng. 118, 1–14. https://doi.org/10.1016/j.petrol.2014.03.012.

Ma, W., Yang, Z., Yi, X., et al., 2008. Current progresses on laser drilling technology. Oil Field Equip. 11, 11–17 (in Chinese).

Nath, A.K., 2014. Laser drilling of metallic and nonmetallic substrates. Compr. Mater. Process. 115–175. https://doi.org/10.1016/B978-0-08-096532-1.00904-3.

Ndeda, R., Sebusang, S.E.M., Marumo, R., et al., 2017a. On the role of laser pulses on spallation of granite. Lasers Manuf. Mater. Process. 4 (2), 60–75. https://doi.org/10.1007/s40516-017-0037-z.

Ndeda, R.A., Sebusang, S.E., Marumo, R., et al., 2017b. Numerical model of laser spallation drilling of inhomogeneous rock. IFAC-PapersOnLine 50 (2), 43–46. https://doi.org/10.1016/j.ifacol.2017.12.008.

Olson, J.J., Olson, K.S., 1975. ARPA-Bureau of Mines Rock Mechanics and Rapid Excavation Program, A Research Project Summary. ARPA-Bureau of Mines Rock Mech. Rapid Excav. Progr.

Pan, H., Hu, Y., Kang, Y., et al., 2021. Impact of dynamic swelling increment factor on coal permeability. Arabian J. Geosci. 14 (16), 1652. https://doi.org/10.1007/s12517-021-08091-2.

Pan, H., Hu, Y., Kang, Y., et al., 2022. The influence of laser irradiation parameters on thermal breaking characteristics of shale. J. Petrol. Sci. Eng. 213, 110397. https://doi.org/10.1016/j.petrol.2022.110397.

San-Roman-Alerigi, D.P., Batarseh, S.I., 2016. Numerical modeling of thermal and mechanical effects in laser-rock interaction – An overview. 50th U.S. Rock Mech. Geomech. Symp.

Siegesmund, S., Sousa, L., Knell, C., 2018. Thermal expansion of granitoids. Environ. Earth Sci. 77 (2), 41. https://doi.org/10.1007/s12665-017-7119-2.

Wang, Y., Shi, Y., Jiang, J., et al., 2019. Experimental study on modified specific energy, temperature field and mechanical properties of Xuzhou limestone irradiated by fiber laser. Heat Mass Tran. 56 (1), 161–173. https://doi.org/10.1007/s00231-019-02682-2.

Xu, Z., Reed, C.B., Parker, R.A., et al., 2002. Laser rock drilling by a super-pulsed CO_2

laser beam. ICALEO® 2002: 21st International Congress on Laser Materials Processing and Laser Microfabrication. https://doi.org/10.2351/1.5065633.
Xu, Z., Reed, C.B., Konercki, G., et al., 2003. Specific energy for pulsed laser rock drilling. J. Laser Appl. 15 (1), 25–30. https://doi.org/10.2351/1.153664.
Xu, Z., Reed, C., Parker, R., et al., 2004a. Laser spallation rocks for oil well drilling. In: 23rd International Congress on Applications of Lasers and Electro-Optics. https://doi.org/10.2351/1.5060237.
Xu, Z., Reed, C.B., Graves, R., et al., 2004b. Rock perforation by pulsed Nd:YAG laser. Int. Congr. Appl. Lasers Electro-Opt. vol. 1406. https://doi.org/10.2351/1.5060219.
Xu, Z., Yamashita, Y., Reed, C., 2005. Modeling of laser spallation drilling of rocks for gas and oil well drilling. SPE Techn. Conf. Exhib. https://doi.org/10.2118/95746-MS.
Zhang, Y., Shen, Z., Ni, X., et al., 2014. Modeling and simulation on long pulse laser drilling processing. Int. J. Heat Mass Tran. 73, 429–437. https://doi.org/10.1016/j.ijheatmasstransfer.2014.02.037.
Zhang, T., Jia, Z., Cui, H., et al., 2016. Analysis of melt ejection during long pulsed laser drilling. Chin. Phys. B 25 (5). https://doi.org/10.1088/1674-1056/25/5/054206.
Zhao, Z., Li, X., He, J., et al., 2018. A laboratory investigation of fracture propagation induced by supercritical carbon dioxide fracturing in continental shale with interbeds. J. Petrol. Sci. Eng. 166, 739–746. https://doi.org/10.1016/j.petrol.2018.03.066.